Cyclic olefin polymer membrane as an emerging material for CO$_2$ capture in gas-liquid membrane contactor

Malihe Sabzekar[a], Mahdi Pourafshari Chenar[a,**], Mohamed Khayet[b,c,*], Carmen García-Payo[b], Zahra Maghsoud[a], Marcello Pagliero[d]

[a] *Department of Chemical Engineering, Faculty of Engineering, Ferdowsi University of Mashhad, Mashhad, Iran*

[b] *Department of Structure of Matter, Thermal Physics and Electronics, Faculty of Physics, University Complutense of Madrid, Avda. Complutense s/n, 28040 Madrid, Spain.*

[c] *IMDEA Water Institute, Avda. Punto Com nº 2, 28805 Alcalá de Henares, Madrid, Spain.*

[d] *Membrane&membrane Research Group, Department of Chemistry and Industrial Chemistry, University of Genoa, via Dodecaneso 31, 16146, Genoa, Italy*

* Corresponding author.

Phone: +34-91-3945185; E-mail: khayetm@fis.ucm.es (M. Khayet)

* *Corresponding author. E-mail: Pourafshari@um.ac.ir (M. Pourafshari Chenar)

Abstract

Porous flat sheet membranes were prepared with a commercial grade of cyclic olefin polymer (COP) for CO_2 capture using membrane contactor (MC). The membranes were prepared via non-solvent induced phase separation technique using different types of additives, namely, polyvinylpyrrolidone (PVP), polyethylene glycol (PEG400) and sorbitan monooleate (Span 80), and coagulants (acetone and 70/30 wt% acetone/water mixture) were investigated. The prepared membranes were characterized in terms of the thickness (70 - 85 µm), porosity (50 - 80%), mean pore size (158 - 265 nm), bubble pore size (~ 0.6 - 12 µm), liquid entry pressure (1.67- 4.55 bar), water contact angle (~ 94º - 111º), monoethanolamine (MEA) contact angle (~ 67º - 73º) and mechanical properties (tensile strength: 4.53 – 5.15 MPa, elongation at break: 4 – 8% and Young´s modulus: 190 – 232 MPa). The thermodynamic study of COP membranes proved that a fast phase inversion of the proposed system resulted in a more porous structure. The addition of PEG400 and Span 80 caused delayed demixing and influenced the morphological structure and MC performance. The structural and topographical characteristics of the membranes were also studied. The CO_2 absorption test performed at 27 ºC showed that the maximum CO_2 absorption flux was around 16×10^{-5} mol/m^2.s using 1M MEA aqueous solution as absorbent with fixed liquid and gas flow rates at 150 L/h and 8.4 L/h, respectively. It was found that the considered additives enhanced the MC performance and affected the CO_2 absorption flux.

1

1. Introduction

Global warming and climate change, which arise from carbon dioxide (CO_2) emission as the most predominant greenhouse gas, have driven world's attention to CO_2 capture. The conventional gas absorption methods including packed tower, spray tower, bubble column, etc., possess some drawbacks including low gas loading capacity, large equipment size, high energy consumption and initial investment cost. Liquid absorption allocates more than 90% of the market among the different methods of CO_2 capture and accordingly amine-based CO_2 absorption column has been extensively used at industrial scale. However, foaming and liquid channeling are two major operating problems in solvent absorption columns [1].

Membrane contactor (MC) technology, as a well-understood and promising alternative technology to conventional gas-liquid contactors, provides an attractive possibility to capture CO_2 via combined chemical absorption and membrane processes. This technology involves mass transfer of CO_2 through a porous and non-selective membrane, which serves as an interfacial barrier, and finally is chemically absorbed into the liquid absorbent. In addition, MC technology offers relatively some advantages including high gas-liquid interfacial area per unit volume, less energy consumption, flexible operation, low cost, independent control of gas and liquid flow rates, easy installation, scale up and simple maintenance [2, 3].

The membrane as the main component for MC application should fulfill some essential requirements such as a high surface porosity (high permeable membrane) to increase the contact area between gas and liquid phases, high hydrophobicity with small pore size to minimize wetting, low mass transfer resistance, and excellent chemical resistance to various liquid absorbents [4]. Additionally, it was expressed that a membrane with low surface porosity and small pore size is more stable to wetting than a membrane with high porosity and large pore size [5].

The most common traditional membrane materials for MC membrane engineering are inherently hydrophobic polymers including polyethylene (PE), polypropylene (PP), polytetrafluoroethylene (PTFE), polyvinylidene fluoride (PVDF) as well as the co-polymer poly (vinylidene fluoride-co-hexafluropropylene) (PVDF-HFP). Since PP and PE are inexpensive and their modules are commercially available, they have often been used in MC. However, they suffer from wetting by some low interfacial tension absorbents and are only made by thermal methods since they are not soluble in most solvents. Fluorine-containing polymeric membranes like PVDF and PTFE membranes are more hydrophobic and show better gas absorption performance compared to PP and PE, but they are expensive [6]. Many attempts were also reported in testing different membrane materials including polyetherimide (PEI) [7], polysulfone (PSf) [8], poly (phenylene oxide) (PPO) [9], polyacrylonitrile (PAN) [10], poly (vinyl chloride) (PVC) [11] and polyether ether ketone (PEEK) [12] in different MC applications. In this regard, the development and/or selection of an appropriate membrane material for MC membrane formation seems to be necessary.

Cyclic olefin polymers (COP) are promising groups of polymers for MC membrane engineering because of their inherent properties and appropriate processability. After the discovery of the cyclic olefin polymer synthesized from ring-opening polymerization, they were commercialized as ZEONEX®, marketed in 1991, and ZEONOR®, marketed in 1998. Cyclic olefin polymer is an amorphous polyolefin with a bulky ring structure in the main chain, synthesized from Norbornene (Fig. 1) [13]. This has a rigid bridged-ring structure that prevents crystallization. The combination of their relatively low price, high transparency, low water absorption ($< 0.01\%$) even in high humidity environment, biocompatibility, good mechanical strength, high chemical resistance to hydrolysis by acids and alkaline agents as well as to polar solvents make them an ideal candidate for various fields including packaging, optics and medical equipment. In addition, COP shows outstanding properties including high heat

resistance, low specific gravity, viscosity and thermal conductivity coefficient (0.12-0.15

W/m.K), and very good melt processability [14,15].
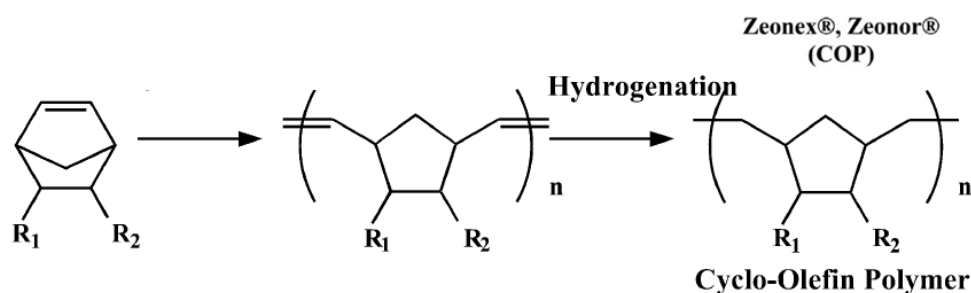
Fig. 1. Cyclic olefin polymer synthesis from norbornene [13]**.**

It is worth quoting that there are few documentations about COP application in membrane

technology. Hu et al. [16] investigated for the first time the gas transport and sorption

properties of the cyclic olefin copolymer (COC), the copolymer of ethylene and norbornene,

with different norbornene contents. The performance of dense COC membranes was strongly

affected by the norbornene content in the polymer matrix (i.e. more norbornene content resulted

in more fractional free volume and increase of gas solubility and permeability). Based on their

results, the sorption level of CO_2 was higher than O_2 and N_2 and attractive CO_2 permeability

and O_2/N_2 ideal selectivity values were achieved [16]. Doğu and Ercan [17] prepared COC

composite membranes by melt processing method using a twin screw extruder and various

types of graphite nano-sheets as additives. It was reported that introducing low amounts of two-

dimensional (2D) graphitic nano-sheet into the thermoplastic matrix resulted in high

performance membranes with enhanced H_2/CO_2 and H_2/CH_4 selectivities compared to other

conventional mixed matrix membranes and the current permeability/selectivity tradeoff

(Robeson's 2008 upper bound) was also surpassed for H_2/CO_2 [17]. Shutova et al. [18]

synthesized a novel highly permeable glassy polynorbornene to form a dense membrane. The

desorption of CO_2 from a typical absorption liquid (30 wt% diethanolamine (DEA) in water)

containing dissolved CO_2 was conducted under a high-pressure/temperature gas-liquid

1   membrane contactor at 100 ºC. Apart from the good chemical stability and the high barrier

2   properties for a number of alkanolmines, this membrane exhibited high gas permeability as a

3   result of its high fractional free volume. A stable performance of this dense membrane in

4   membrane contactor was confirmed [18]. In our previous study, porous COP membranes were

5   successfully prepared for membrane distillation (MD) application [19]. It is to be noted that

6   both MD and MC membranes share common characteristics such as their high porosity, liquid

7   entry pressure (*LEP*) and water contact angle with narrow pore size distributions in the range

8   of few hundred nanometers. In addition, some superior properties of COP polymer such as its

9   low water absorption and high chemical resistance seem to be very useful in membrane

10   contactor (MC) applications. The structure of norbornene causes a reasonably high free volume

11   in membrane structure that may affect the CO_2 permeability [18]. To the best of our knowledge

12   there is no publication concerning the development of porous COP membranes for MC

13   applications.

14   In the present study, COP membranes were prepared via non-solvent induced phase

15   separation (NIPS) method using different additives, polyvinylpyrrolidone (PVP), polyethylene

16   glycol (PEG400) and sorbitan monooleate (Span 80), and two coagulants, acetone and 70/30

17   wt% acetone/water mixture. The characteristics of the prepared membranes were compared

18   with those of membranes commonly used in MC. Finally, the performance of COP membranes

19   was examined in MC application for CO_2 absorption using 1M monoethanolamine (MEA)

20   aqueous solution and the obtained results were compared with other MC membranes.

21   **2. Experimental**

22   *2.1 Materials and membrane preparation*

23   The used polymer, chemicals, solvent and non-solvent along with the corresponding

24   suppliers are listed in Table 1.

Table 1. The list of used polymer, chemicals and solvents.

No.	Material	Performance	Supplier
1	COP (ZEONEX® 480R) [*] (Mw: 480000 g/mol)	polymer	Zeon Europe GmbH (Germany)
2	Polyethylene glycol (PEG) (*Mn*: 400 g/mol)	Hydrophilic additive	Sigma-Aldrich
3	Polyvinylpyrrolidone K90 (PVP) (Mw: 360,000 g/mol)	Hydrophilic additive	Fluka Chemie AG
4	Sorbitan monooleate (Span® 80)	Nonionic surfactant	Sigma-Aldrich
5	Chloroform	Solvent	Acros Organics
6	Acetone	Non-solvent	Acros Organics
7	POREFIL®	Wetting liquid	Porometer
8	Isopropyl alcohol (IPA)	Wetting liquid	Sigma-Aldrich
9	Monoethanolamine (MEA)	Liquid absorbent	Sigma-Aldrich
10	CO_2/ N_2 gas mixture	gases	Air Liquide

[*] COP properties (T_g: 137 °C, density: 1.01 g/cm^3, Melt Flow Index (MFI); 21 g/10 min obtained under a load of 2.16 kg at 280 °C).

A constant amount of each additive (0.2 wt%) was mixed with the solvent (chloroform) using a magnetic stirrer at 120 rpm at room temperature (22 °C) for about 1 h, followed by the addition of 10 wt% of the polymer (COP) in the solution. For porous membrane preparation, two commonly used additives (PVP and PEG400) along with the surfactant (Span 80) were tested to evaluate their role as pore former and investigate the characteristics and the MC performance. The polymer solution was placed in an orbital shaker at 40 °C and 100 rpm until

a homogeneous dope solution was achieved. The degassed polymer dope solution was cast on

a flat glass at room temperature via automatic film applicator (Elcometer 4340, Elcometer®)

while the knife gap and its velocity were set at 0.25 mm and 100 mm/s, respectively. The cast

film was immediately immersed in the non-solvent coagulation bath (acetone with/without

water) at room temperature and left overnight. After taking out and rinsing the flat-sheet

membrane with acetone/water to remove any residual solvent/non-solvent additives, the

membrane was air-dried for 24 h. The prepared membranes together with the corresponding

composition of the used dope solutions and the coagulants are presented in Table 2. The

membrane code M-X-Y means a COP membrane (M) prepared with 0.2 wt% additive X (NA

without additive, PVP, PEG or Span) in the solvent chloroform and the coagulant Y (Acetone

A or acetone/water mixture A/W, 70/30 wt.%).

Table 2. Prepared membranes together with the corresponding dope solution compositions and coagulants.

Membrane code	additive	Additive content (wt%)	Solvent content (wt%)	Coagulant
M-NA-A	No additive	---	90	Acetone
M-PVP-A/W	PVP	0.2	89.8	Acetone/water[a]
M-PEG-A	PEG	0.2	89.8	Acetone
M-PEG-A/W	PEG	0.2	89.8	Acetone/water[a]
M-Span-A	Span 80	0.2	89.8	Acetone

[a] 70/30 wt% in all experiments.

2.2 Cloud point measurement

The ternary phase diagram of the used system (polymer/solvent/non-solvent) with and without additives was studied to understand the thermodynamic behavior of the phase inversion membrane formation process. For this study, polymer solutions with a polymer concentration of 1, 3, 5, 7, and 10 wt% in the solvent were prepared without any additive. To study the effect of the additive on the thermodynamic behavior of the polymer solution, two types of additives, Span and PEG, were considered. The additive concentration in the polymer solution prepared with 10 wt% polymer was maintained at 0.2 wt%. The cloud point was determined by the turbidimetric titration method at the same temperature (35 ℃). For this purpose, 20 µL of each non-solvent (i.e. acetone or acetone/water) was added stepwise to the polymer solution under a constant agitation. For high polymer concentrations where local precipitation occurred, agitation was continued until the solution became homogenous again. Therefore, the necessary quantity of non-solvent tuning the polymer solution permanently turbid was regarded as the cloud point.

2.3 Membrane characterization

The surface and cross-section morphological structure of the COP membranes were examined by a field emission scanning electron microscope (FE-SEM, MIRA3 TESCAN, Czech Republic). The cross-section of the samples was obtained by fracturing the membrane samples in liquid nitrogen. Both the surface and cross-section of the membrane samples were sputter-coated by a thin gold layer of approximately 5 nm using a rotary-pumped sputter coater (Q150R ES, Quorum, England) during 60 s under 20 mA.

The thickness of the membranes was measured using a micrometer equipped with a feeler (ISL Isocontrol). The average value of 30 measured results at different spots of each sample was reported.

The void volume fraction (i.e. porosity, ε) of the flat-sheet membranes was determined by measuring the density of the polymer material (ρ_{pol}) using isopropyl alcohol (IPA) and the density of the membrane (ρ_m) using distilled water as explained elsewhere [20]. The average of three different measurements for each membrane was reported along with their standard deviations.

The *LEP* of distilled water was measured using the experimental setup detailed elsewhere [21]. The pressure was applied gradually by means of a nitrogen cylinder on the container filled with distilled water. The minimum hydrostatic pressure applied on the flat-sheet membrane before water penetrates inside the membrane pores was reported as the *LEP*. These measurements were carried out using three different membrane samples from different batches and the average values together with their standard deviations were reported.

To check the hydrophobic character and wetting resistance of the membranes, the water contact angle (WCA) and MEA contact angle (MCA) were measured in static mode at room temperature using a computerized optical system CAM100, equipped with a CCD camera, frame grabber and image analysis software CAM200usb. More information can be found elsewhere [20]. A Hamilton stainless steel needle was used to control the volume of the droplet of distilled water and 1M MEA (~12 - 14 µL). Five images were recorded during 4 s for each droplet and at least 10 drops were considered for each membrane sample to determine the average θ value together with its standard deviation.

The bubble pore size, the mean pore size and the small pore size of the membranes were determined via the wet/dry flow method using the gas-liquid displacement Porometer and its corresponding computer software (POROLUX™ 100, Porometer). First, the flat-sheet membrane was wetted by a wetting liquid (POREFIL®, surface tension of 16 mN/m) and then, the S-shaped wet curve was obtained by plotting the air flow rate as a function of the applied hydrostatic pressure difference (0 – 0.7 MPa) at room temperature (23 °C). Subsequently, the

1   air flow rate at different hydrostatic pressures through the dry sample was measured to obtain

2   the dry curve. The mentioned parameters were calculated from the obtained cumulative filter

3   flow (CFF) and the differential filter flow (DFF) curves. For each membrane, at least three tests

4   were performed. The complete followed procedure was described elsewhere [21].

5   The mechanical properties of the membranes, including the tensile strength, the elongation

6   at break and the Young's modulus were measured according to the ASTM D 882 specification

7   using an universal tensile tester (SANTAM STM20) equipped with a 6 N load cell at room

8   temperature and a crosshead speed of 5 mm/min with an initial length of 50 mm. The tensile

9   test of each membrane was repeated at least for five samples, and the final mechanical

10   characteristics are reported as the average of the performed measurements.

11   In order to investigate the surface topography and roughness parameters (R_a and R_q) of both

12   the top and bottom surfaces of the COP membranes, the atomic force microscopy (AFM) was

13   carried out using the AFM, Ara research, model: Full plus. The mean roughness (R_a) is the

14   arithmetic average of the absolute values of the surface height deviations measured from the

15   mean plane, while the root mean square roughness (R_q) is the standard deviation from the mean

16   surface plane. The AFM measurements were conducted at room temperature over a scanning

17   area of 5µm×5µm.

18

19   *2.4 CO_2 absorption test*

20   The CO_2 absorption test was carried out using the membrane contactor schematized in Fig.

21   2. A counter-current flow was used for the gas and liquid absorbent. Moreover, Fig. 3 shows

22   the structural diagram of the used plate-and-frame membrane module. The feed gas

23   composition was 15 % (v/v) of CO_2 in N_2, circulating over a membrane with an effective area

24   of 32.6 cm^2 while the 1M monoethanolamine (MEA) aqueous solution was used as absorbent.

25   The liquid and gas flow rates measured by a rotameter and a bubble flowmeter were fixed at

1 150 L/h and 8.4 L/h, respectively. For all experiments, the hydrostatic transmembrane pressure

2 and temperature were set at 5 mbar and 27±1 °C, respectively. CO_2 concentration in the effluent

3 was measured by a gas chromatograph (GC) (Perkin-Elmer Autosystem GC equipped with a

4 TCD). The membranes were tested in both sides (side A: top surface of the membrane sample

5 facing the liquid adsorbent while the bottom surface was brought into contact with the

6 sweeping gas, and side B: bottom surface facing the liquid absorbent while the top surface was

7 brought into contact with the sweeping gas).
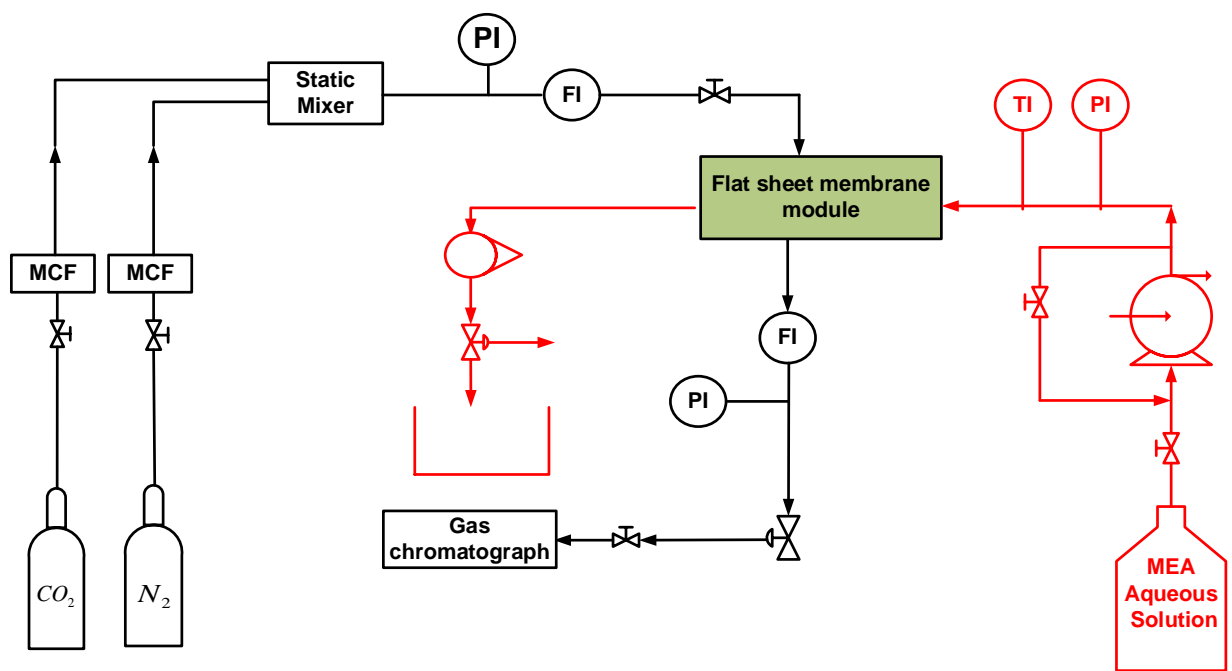
8

9 **Fig. 2.** Schematic of the MC experimental setup for membrane gas absorption.
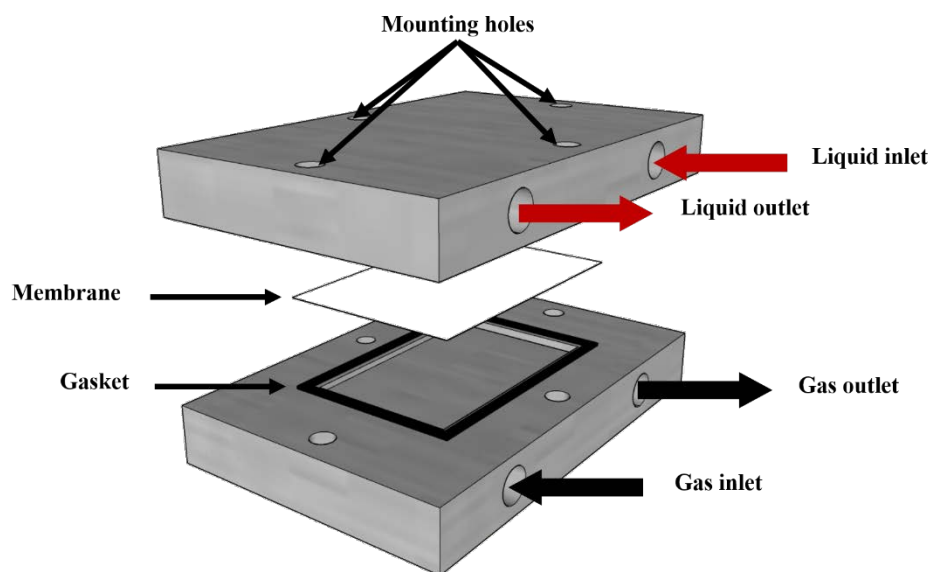
**Fig. 3.** Plate-and-frame membrane module.

3. Results and discussion

3.1 Thermodynamic properties of polymer solutions

The thermodynamic behavior of COP solution during phase inversion process was represented in the isothermal ternary phase diagram (Fig. 4(a-c)). Generally, the precipitation rate of the polymer solution is an important parameter affecting the membrane structure formation. A faster precipitation rate results in more porous and anisotropic structure [22]. According to the cloud point curve (Fig. 4(a)), it was found that the precipitation rate of COP solution is faster compared to PVDF, a common polymer for MC membrane formation [23], provided that the obtained data points in Fig. 4(a) were very close to the COP-chloroform axis. Therefore, a more porous structure was expected for COP phase inversion membrane formation. By decreasing the polymer concentration from 10 to 1 wt%, the cloud point tended to shift progressively away from the COP/solvent axis indicating that a larger amount of acetone was required to induce polymer precipitation. In fact, the increase of COP

1 concentration reduced the thermodynamic stability of the polymer solution and consequently

2 favored the instantaneous liquid demixing. Taking into consideration that a highly porous

3 structure of COP membranes is favorable for MC applications, a COP concentration of 10 wt%

4 showing a faster precipitation rate and consequently more porosity was selected for further

5 experiments and membrane formation.

6 The impact of different additives (Span and PEG) on the miscibility area of the studied

7 system and precipitation rate of the polymer solution is shown in Fig. 4(b). Taking into account

8 the turbid solution containing PVP, the system used for M-PVP-A/W membrane formation was

9 not investigated in terms of its cloud point. It is known that the addition of some additives

10 reduces the miscibility area, promotes phase separation and increases the precipitation rate of

11 the polymer solution tending to form a finger-like structure. However, the addition of additives

12 (PEG and Span) to COP polymer solution shifted the cloud point data toward the non-solvent

13 corner (Fig. 4 (b)). It means that a larger quantity of acetone was needed for COP precipitation

14 indicating delayed phase inversion process and consequently the suppression of finger-like

15 structure may be observed. This result also agrees with the R_{HSP} calculated in our previous

16 study [19], which indicated better affinity of PEG to solvent than to non-solvent and finally the

17 delayed phase inversion and suppression of macrovoids occurred. Span had less affinity to

18 solvent than to acetone compared to PEG. Therefore, its corresponding cloud point data shifted

19 only slightly toward the non-solvent corner than that corresponding to PEG.

20 The addition of 30 wt% of water to acetone exerted a significant effect on the thermodynamic

21 behavior of the phase inversion process as shown in Fig. 4(c). The cloud point of the polymer

22 solution with PEG as additive shifted towards the COP/solvent axis indicating that less non-

23 solvent was required to precipitate the polymer solution. Therefore, an instantaneous phase

24 separation occurred compared to COP solution without additive Finally, the finger-like

25 structure may be expected using acetone/water as non-solvent.

(a)   **(b)**   **(c)**
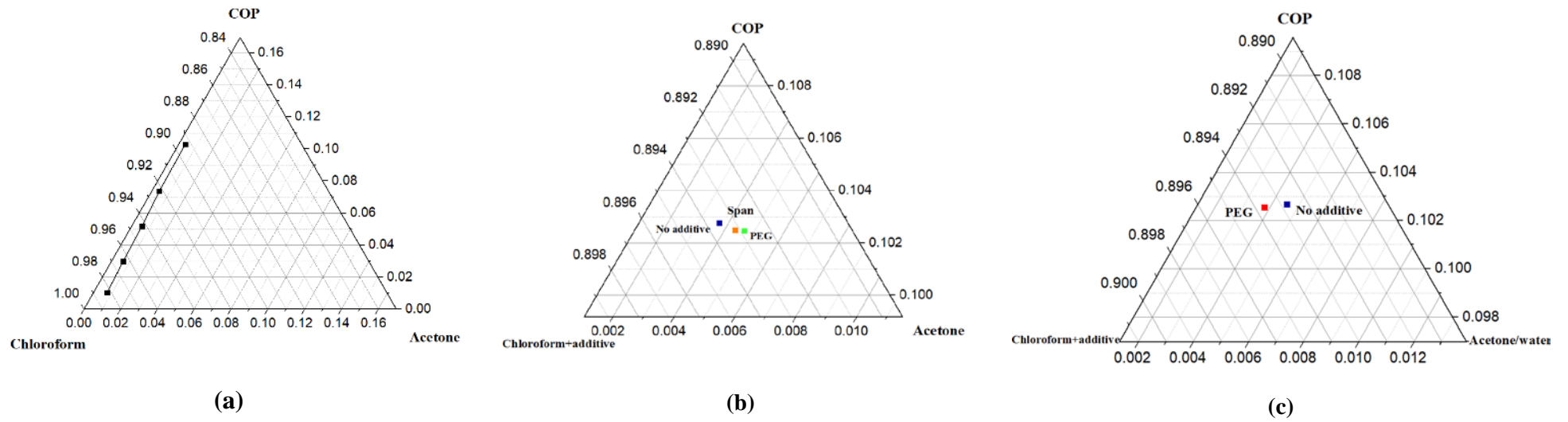
1   **Fig. 4.** Isothermal ternary phase diagram of COP/Chloroform with and without additive/non-solvent systems: (a) different COP concentrations: 1, 3, 5, 7,

2   and 10 wt%; (b) different additives (Span and PEG), and (c) different coagulants (acetone and acetone/water).

3.2 Morphological structure of the membranes

The FESEM images of the top (polymer/air interface), bottom (membrane side facing the glass plate), and cross section of the prepared COP membranes with different additives are shown in Fig. 5. The first visual inspection of the membranes indicated that the membrane M-NA-A prepared without any additive exhibited big macrovoids and all membranes had a top porous structure and an asymmetric cross-section configuration including both finger-like and sponge-like structures. It is worth mentioning that the final morphology of the membranes depended on the domination of delayed or instantaneous demixing. As it was found from the thermodynamic experiments, the precipitation rate of COP membranes (10 wt%) was fast indicating an instantaneous demixing. The pores at the bottom surface of the membranes were larger than those of the top surface due to the slower phase inversion occurred near the glass-touching side of the membrane. The structure of the COP membranes depended on the phase separation rate influenced by the complex correlation between the thermodynamic enhancement and the rheological hindrance, which consequently caused either induced or suppressed macrovoid formation through the cross-section of the membranes [24]. The addition of the PVP additive induced the enhancement of demixing as a result of the thermodynamic instability leading to the increase of finger-like macrovoids (b-series in Fig. 5). This observation was also suggested by Nabian et al. [25] indicating that the addition of PVP in the polysulfone polymeric solution changed the membrane structure from sponge-like to finger-like structure, in water coagulant, and consequently improved the CO_2 absorption flux.
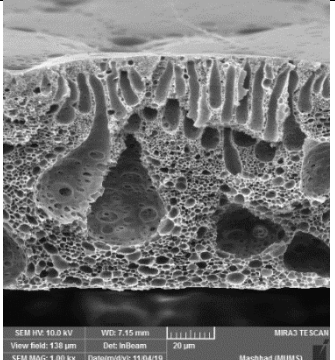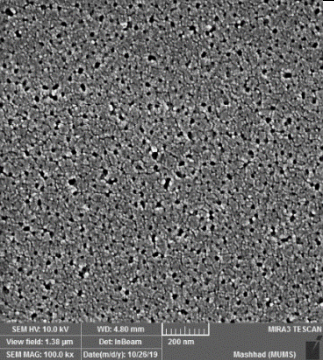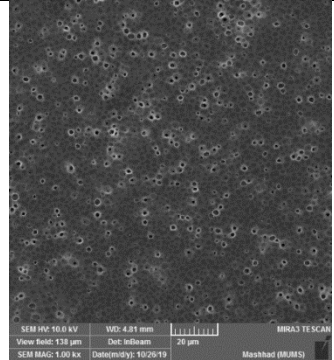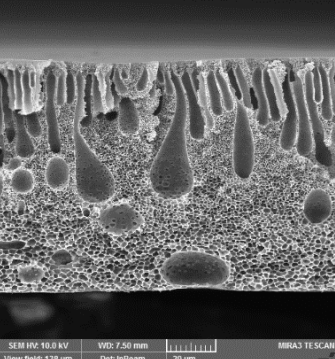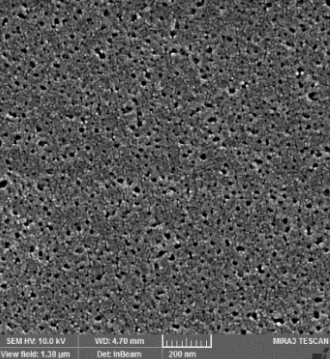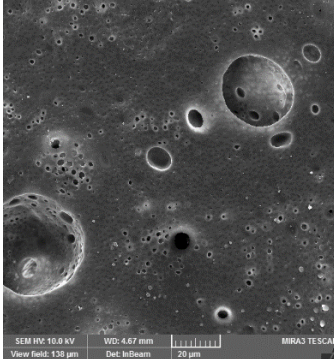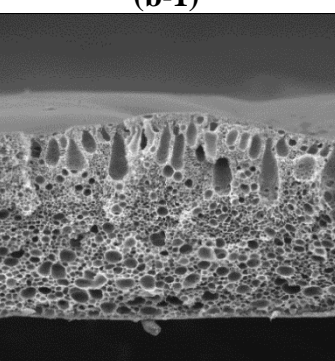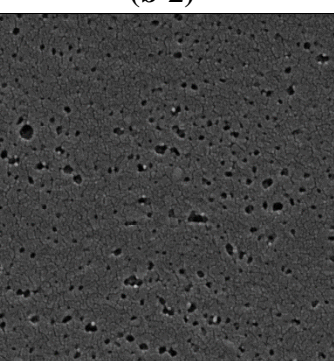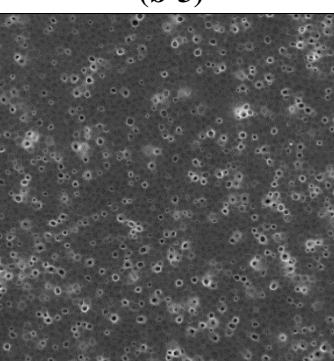
According to some studies, the general effect of PEG additive was the suppression of macrovoids and the creation of a honeycomb structure together with free porous interconnecting channels in a sponge-type matrix [26]. This has also been proved in this study as can be seen in Fig. 4 (b) and 5 (c-1). According to thermodynamic experiments, the addition
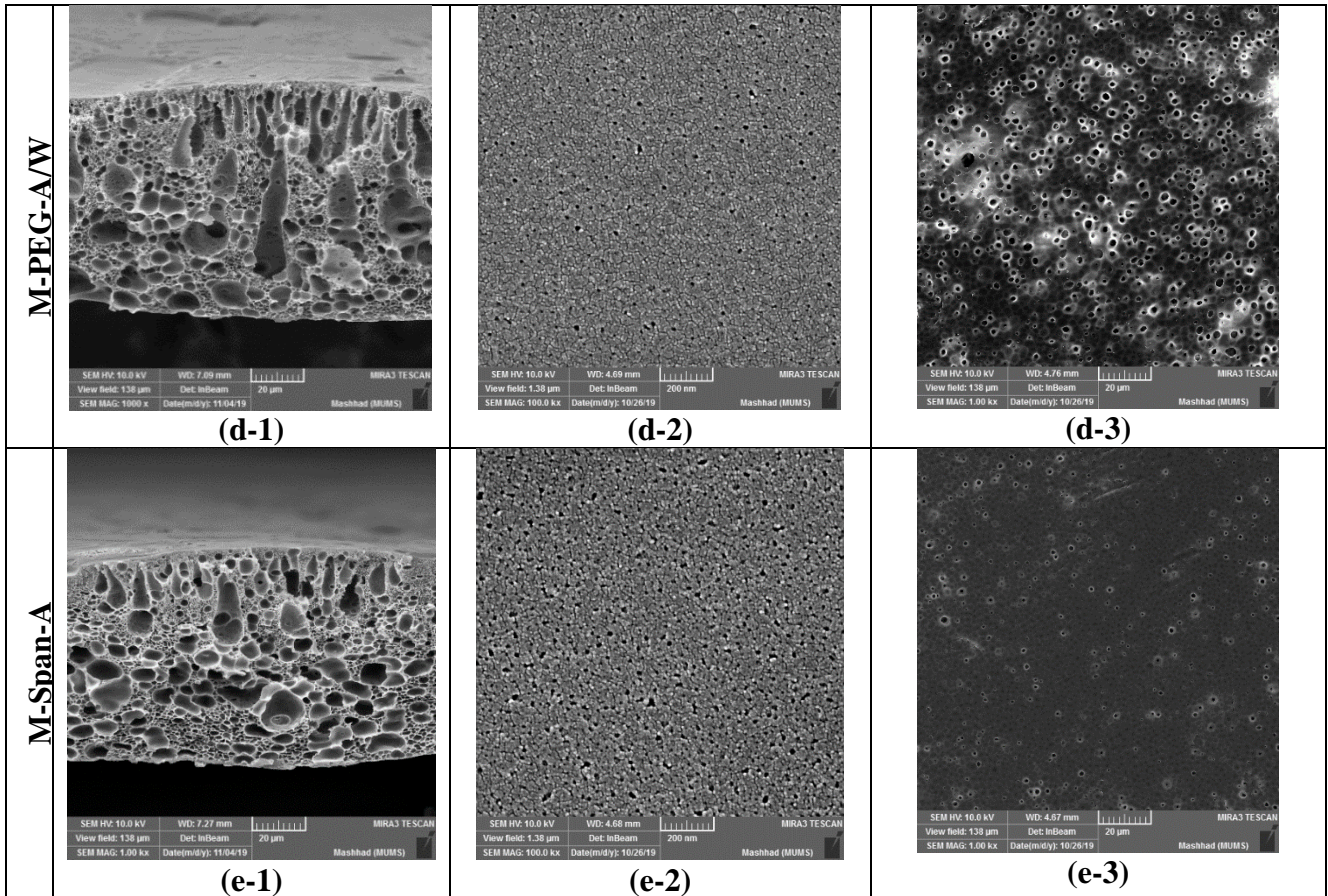
of PEG made the cloud point shift towards the COP/acetone axis indicating that more non-solvent was required to induce the polymer precipitation. Thus, the domination of delayed demixing caused the suppression of the macrovoids. The effect of the coagulant type on the COP membrane structure was also studied when using the PEG additive (i.e. M-PEG-A and M-PEG-A/W membranes, c-series and d-series in Fig. 5). With the addition of water to acetone, big macrovoids appeared through the membrane cross-section and the porosity of the bottom surface was increased (d-3 in Fig. 5). This difference may be explained by the solubility parameters of the COP polymer and the coagulants. In fact, the solubility parameter difference of acetone/water (26.4 $MPa^{0.5}$) toward COP (18.3 $MPa^{0.5}$) is higher than that of acetone (19.9 $MPa^{0.5}$) toward COP. Therefore, acetone/water is a stronger non-solvent than acetone, causing a rapid demixing (i.e. a fast phase separation) and macrovoids formation [27]. This result also agrees with the obtained cloud point data (Fig. 4 (c)) in which the system used for the formation of PEG containing membrane required less acetone/water coagulant to induce polymer precipitation and promote a phase inversion process favorable for finger-like structure.

Span 80 with a hydrophile-lipophile value (HLB) of 4.3 and a greater hydrophobic character than PEG and PVP was also considered as an additive for pore formation in COP membrane matrix. As shown in Fig. 5 (e-series), a lot of macrovoids appeared across the COP membrane structure along with short finger-like structure at the top membrane surface. On the other hand, the porosity of the bottom surface of the membrane was decreased. As it was shown in Fig. 4 (b), the addition of Span to the COP polymer solution resulted in a more stable casting solution and consequently more acetone was required to disturb the system equilibrium compared to the system used for M-NA-A membrane formation. As a result, a delayed phase separation occurred inducing reduced lengths of the formed finger-like structure. In addition, the formation of drop shape-like cavities in the sponge-like layer can also be associated to the slow precipitation rate of the COP polymer solution. This result agrees with Ge et al. [28] who

1   claimed that the addition of low HLB surfactant to the polymer solution caused a more stable

2   casting solution and decreased the phase separation rate. As a result, the finger-like structure

3   was decreased and the sponge-like structure showed bigger pores.

	Cross section (×1000 magnification)	Top surface (×100,000 magnification)	Bottom surface (×1000 magnification)
M-NA-A	(a-1)	(a-2)	(a-3)
M-PVP-A/W	(b-1)	(b-2)	(b-3)
M-PEG-A	(c-1)	(c-2)	(c-3)

Fig. 5. FESEM images of the prepared COP membranes with (PVP, PEG and Span) and without
additives using different coagulants (acetone and acetone/water mixture).

3.3 Characteristics and mechanical properties of COP membranes

Table 3 summarizes the measured characteristics (Thickness, δ; porosity, ε; *LEP*; water
contact angle, WCA; MEA contact angle, MCA; mean and bubble pore size) and the
mechanical properties (tensile strength, σ_b; elongation at break, ε_b; and Young´s modulus, E))
of the prepared COP membranes. Based on the obtained results, the M-NA-A was the thickest
membrane while the M-PVP-A/W was the thinnest one. In general, taking into consideration
the obtained standard deviations, no significant difference could be detected between the
thickness of all prepared membranes.

One of the important properties in MC application is membrane porosity, which dictates the free space for mass diffusion. Generally, a higher porosity results in a higher membrane mass transfer coefficient (i.e. a higher porosity facilitates the gas transport in MC [7]). Based on the obtained results, the M-NA-A and the membranes prepared with PVP membranes were highly porous (~80%) due to the much faster phase inversion mechanism compared to the other prepared membranes. The addition of the two types of additives (PEG and Span) resulted in a lower void volume fraction. This is attributed to the reduction or suppression of the macrovoids observed through the cross-section of the mentioned membranes.

For PEG additive, the decrease of the porosity was more pronounced when the coagulant was acetone/water mixture. As stated previously, acetone/water mixture is a stronger coagulant for COP than acetone alone, so the initial solvent and non-solvent demixing creates a less permeable layer that hindered an easy diffusion of the non-solvent into the polymer solution during membrane formation, resulting in smaller membrane surface pores and lower porosity [29,30]. The same result was obtained for the membrane M-Span-A showing a porosity of 50%. According to the Lin et al. [31], who investigated the effect of a wide range of surfactants with various HLB values, surfactants with higher HLB values are more effective to instantaneous demixing inducing macrovoids when a polar coagulant is used. Because acetone is a polar coagulant, the low HLB surfactant may resulted in delayed demixing and consequently suppression of macrovoids as proved previously in Section 3.1. Moreover, it is known that the more thermodynamically stable polymer solution decreases the phase separation rate and the membrane porosity [7]. Taking into consideration that Span caused a delayed demixing (Fig. 4(b)), the decrease of the corresponding membrane porosity was also expected.

The effect of the used additives on the hydrophobic character of the COP membranes was investigated via the measurements of the static water contact angle (WCA). As the MEA

solution was used as absorbent in MC, the static contact angle using 1M MEA solution (MCA) was also measured. The results were also summarized in Table 4. The M-NA-A showed a good surface hydrophobicity with a high water contact angle (111.0±3.2º). As it was expected, the use of the additives, PVP and PEG reduced the WCA. Since PEG is a smaller molecule than PVP, which is more hydrophilic, the WCA of the membrane M-PVP-A/W (93.5º) was less than that of the two COP membranes prepared with PEG (102.9° and 103.8° for M-PEG-A and M-PEG-A/W, respectively). The slightly greater WCA of the membrane M-PEG-A/W compared to that of the membrane M-PEG-A may be due to its higher roughness parameters as it is shown later on. Although the roughness parameters of the membrane M-Span-A was slightly higher than that of the membrane M-NA-A, its WCA was lower. This observation may be attributed to the hydrophilic part of the Span additive. The MCA of all COP membranes was considerably smaller than the WCA due to the strong dependency of the contact angle to the surface tension of the testing liquid. The surface tension of 1M MEA solution (~ 60 mN/m) is lower than that of water (~ 72 mN/m) due to the presence of organic compounds. Therefore, a lower liquid surface tension leads to a lower contact angle with the membrane surface. The same contact angle reduction with MEA solution with respect to that of water was also observed for a PVDF membrane [32]. In general, no significant difference was observed for MCA of COP membranes (67º -73º) if the standard deviations are taken into account. It is worth mentioning that the highest MCA value (~73º) corresponds to the membrane prepared with Span additive compared to the other membranes. This result has a good agreement with the roughness parameters as discussed later on.

It has been reported that membranes used in MC applications have pore sizes ranging from few nanometers to a few hundred nanometers depending on the fabrication method [9, 33]. According to the obtained results shown in Table 3, the addition of PVP led to an increase of the mean pore size compared to the membrane M-NA-A prepared without any additive (265

nm *vs*. 211 nm, respectively, Table 3). As explained by Matsuyama et al. [34], this is due to the hydrophilic character of PVP that promotes pores enlargement through its easy leaching out into the water coagulation bath favoring water inflow and increasing the quench depth across the membrane. On the contrary, the PEG additive reduces the mean pore size (196 nm and 158 for M-PEG-A and M-PEG-A/W, respectively). This can be explained through thermodynamic experiments indicating that the domination of delayed demixing causes suppression of macrovoids. This result was also proved by the structural morphological study illustrated in Fig. 5 (c-1). When using acetone/water mixture as coagulant, the mean pore size was reduced while the bubble pore size was increased (1560 nm for M-PEG-A/W *vs*. 1408 nm for M-PEG-A, Table 3 and Fig. 5, d-1). According to the thermodynamic study (Fig. 4 (c)), a stronger coagulant result in a rapid demixing and some macrovoids appeared in the membrane structure (Fig. 5 (d-1)) increasing therefore the bubble pore size. On the other hand, the addition of water to acetone increased the viscosity of the coagulant affecting the diffusion rate (i.e. kinetic effect), suppressing macrovoids and finally reducing the mean pore size [35]. As mentioned in the thermodynamic study, compared to the membrane M-NA-A, the finger-like macrovoids of the membrane M-Span-A were reduced and its sponge-like structure in the membrane sublayer was changed to big cavities across the membrane as a result of delayed demixing. Therefore, a significant reduction of the bubble pore size of this membrane was observed with the increase of the mean pore size (239 nm, Table 3).

The *LEP* is the minimum pressure needed to wet the maximum membrane pores by the testing liquid, in this case distilled water. In general, *LEP* depends on the hydrophobic character of the membrane, the surface tension of the used liquid, water or absorbent, the maximum pore size and its structure. In MC application, the membrane should have an appropriate *LEP* to prevent liquid penetration into its pores. According to the *LEP* data shown in Table 3, all the prepared membranes have *LEP* values greater than 1.6 bar and are within the range of

membranes commonly used in MC [8,36]. Except for the membrane M-NA-A, all COP membranes showed a gradual decrease of the *LEP* with the increase of the maximum pore size (i.e. bubble pore size), and the membrane M-Span-A exhibited the highest *LEP* value (4.55±0.3 bar). Although the maximum pore size of the membrane M-NA-A is much higher than that of the other membranes, the *LEP* of this membrane is reasonably high due to its greater hydrophobicity.

The mechanical properties (tensile strength, σ_b, elongation at break, ε_b, and Young´s modulus, *E*) of the prepared COP membranes are also presented in Table 3. In general, since the membranes fabricated by NIPS method have macrovoids, their mechanical strength is low as these macrovoids act as stress centralized weak points under an applied force [37]. In this case, the COP membranes showed a tensile strength in the range 4.5- 5.1 MPa, which is suitable for the MC applications as low transmembrane hydrostatic pressures between gas and absorbent phases are normally applied [38]. However, the elongation at break was found to be quite low because of the plastic behavior of COP and its application below its T_g resulting more brittle membranes. Up on the addition of the three additives, both the tensile strength and the elongation at break were enhanced. It is worth quoting that the additives, PVP and PEG, both affect the flexibility of the resultant membranes and consequently better mechanical properties were achieved. Moreover, the reduction of deep cavities with the addition of Span and PEG (Fig. 5) improved the mechanical strength. Young's modulus was also increased except for the membrane M-PVP-A/W due to its larger finger-like structure compared to the other COP membranes. It can be seen that the membrane M-Span-A having the lowest porosity or void volume fraction, possess the highest mechanical strength.

Table 3. Thickness (δ), porosity (ε), *LEP*, water contact angle (WCA), MEA contact angle (MCA), mean and bubble pore size, and mechanical properties (tensile strength, σ_b, elongation at break, ε_b, and Young´s modulus, *E*) of the prepared COP membranes.

| Membrane code	δ (µm)	ε (%)	*LEP* (bar)	WCA (°)	MCA (°)	Bubble pore size (nm)	Mean pore size (nm)	σ_b (MPa)	ε_b (%)	*E (MPa)*
M-NA-A	85±5	80.3±3.3	1.96± 0.19	111.0±3.2	70.5±3.1	11934±141	211±3	4.53±0.02	4.08 ±1.40	208±6
M-PVP-A/W	70±5	79.4±1.5	1.67±0.18	93.5±2.6	66.7±1.6	1599±52	265±6	4.73±0.32	6.76 ±1.70	190±4
M-PEG-A	75±5	75.8±1.8	2.82±0.09	102.9±2.4	67.7±1.0	1408±20	196±8	4.82±0.19	5.44 ±1.79	210.1±7
M-PEG-A/W	75±5	73.3±2.2	2.04±0.14	103.8±1.4	69.9±2.1	1560±35	158±5	5.05±0.04	6.15 ±1.83	222.1±6
M-Span-A	80±5	50 ±1.7	4.55±0.34	100.0±2.2	72.6±5.1	636±10	239±2	5.15±0.29	7.94 ±0.98	232.1±5

3.3 Membrane topography

The three-dimensional surface images and the surface roughness parameters (R_a and R_q) of both the top and bottom surfaces of COP membranes are shown in Fig. 6 and Table 4, respectively. In the topographic AFM images, the dark and bright parts represent the pores and nodules, respectively. In general, the obtained images of the top surface of all membranes were almost similar, except the membrane M-PVP-A/W, which exhibited the highest R_q roughness parameter due to some intensified asperities. The COP membranes prepared with PEG additive (M-PEG-A and M-PEG-A/W) exhibited smoother top surfaces than that of the other membranes prepared with and without additive. This may be attributed partly to their smaller pore size as discussed previously. For the COP membranes prepared with PEG additive, the addition of water to acetone coagulant caused a small increase in roughness parameters (Fig. 6 and Table 4). This observation was also reported by Ahmad et al. [39] who investigated the effect of solvent addition in the coagulation bath. It was also observed that the addition of more solvent in the coagulation bath (>60 wt%) increased the solvent/non-solvent affinity and resulted in a decrease of roughness parameters. It can also be seen that the AFM topography images and roughness parameters (Fig. 6 and Table 4) of the membrane M-Span-A is almost similar to those of the M-NA-A membrane prepared with additive, if the standard deviations are taken into consideration.

For all membranes, the bottom surface was rougher than the top surface due to the effect of the glass plate during membrane formation. In fact, from figures 5 and 6, it can be seen that the size of the pores and nodules of the bottom surfaces were greater than those of the top surfaces.

It is well known that membrane hydrophobicity determined by water contact angle measurement is also related to the surface roughness. In the present study, the COP membrane prepared without any additive showed high water and MEA contact angles (111° and 71°,

respectively). However, their roughness parameters of the top membrane surface were found

to be quite similar to those of the membranes M-PVP-A/W and M-Span-A. According to the

contact angle data, the M-PVP-A/W membrane had the least water and MEA contact angles.

This indicates that the hydrophilic nature of the high molecular weight PVP was responsible

for the reduction of contact angles. The same observation is applied when comparing the

roughness parameters of the membranes M-Span-A and M-NA-A. Taking into account the

obtained standard deviation, the difference of the MCA of these membranes could be

considered insignificant. The lower water contact angle of the membrane M-Span-A may be

associated to the hydrophilic part of the additive Span. In addition, compared to the membranes

prepared with additives, the ones prepared with PEG membranes showed lower roughness

parameters of their top surfaces but higher water contact angles (Fig. 6). Because the PEG size

is smaller than the other used additives, this can be leached out easily during membrane

preparation. Therefore, higher water contact angles were observed for the membranes prepared

with PEG compared to M-PVP-A/W and M-Span-A membranes. Pezeshk et al. [38] reported

that the addition of PEG-200 to PVDF dope solution decrease the pore size and consequently

resulted in surface roughness decrease. The mean pore size of the PEG-modified COP

membranes (Table 3) was the least among other membranes.

Membrane code	Top	Bottom
M-NA-A		
M-PVP-A/W		
M-PEG-A		
M-PEG-A/W		
M-Span-A		
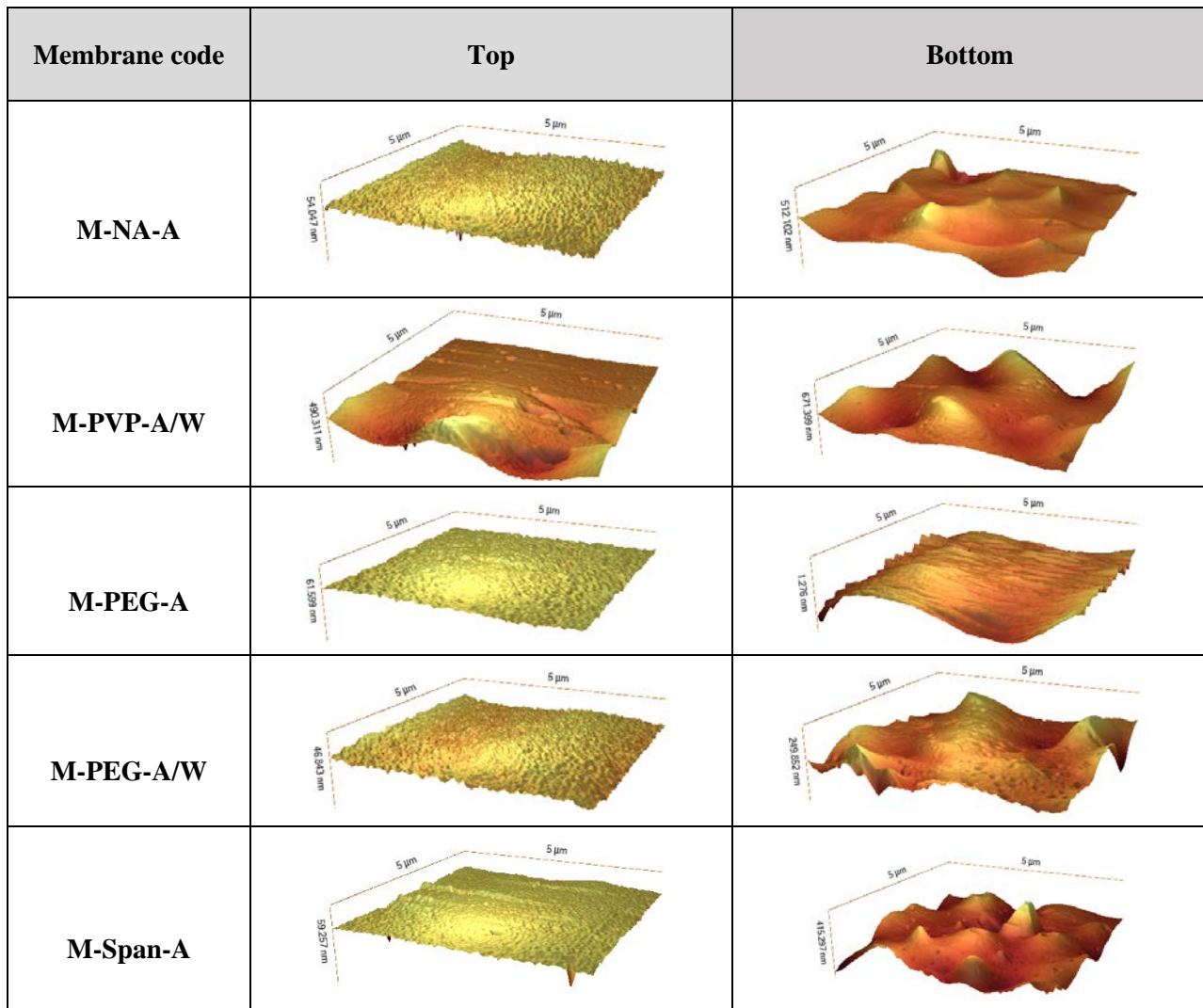
1   **Fig. 6.** 3D AFM images of the top and bottom surfaces of the prepared COP membranes.

2   **Table 4.** Roughness parameters, R_a and R_q, of the prepared COP membranes.

Membrane code	Top		Bottom	
	R_a (nm)	R_q (nm)	R_a (nm)	R_q (nm)
M-NA-A	106.4±3.8	126.7±5.0	108.1±0.5	132.1±4.0
M-PVP-A/W	105.9±10.0	131.4±18.9	237.5±7.2	258.4±5.2
M-PEG-A	81.4±2.0	94.7±2.5	237.2±2.4	278.0±5.3
M-PEG-A/W	99.8±14.0	116.7±12.7	248.8±11.2	298.3±17.5
M-Span-A	107.9±2.8	129.3±4.8	120.3±3.6	152.3±6.5

3

1   *3.4 CO_2 absorption test*

2   The measured CO_2 absorption flux through the membrane contactor is presented in Fig. 7.

3   Since the morphology of both sides of the COP asymmetric membranes are quite different, this

4   test was carried out for both membrane configurations (Side A: top surface contacting the

5   absorbing liquid while the bottom surface was facing CO_2; and side B: bottom surface

6   contacting the absorbing liquid while the top surface was brought into contact with CO_2). The

7   results are plotted in Fig. 7. For the Side A configuration test, all COP membranes had almost

8   the same CO_2 absorption flux except the membrane M-PVP-A/W, which showed a slightly

9   higher flux due to its higher mean pore size. In general, the predominant mass transfer

10   mechanism for membrane gas absorption process is governed by gas diffusion through the

11   membrane pores. Since the diffusion coefficient in large pores is significantly higher than in

12   small ones, larger pore size improves the CO_2 flux in gas absorption application [41]. In

13   addition, Nabian et al. [25] also proved that the addition of PVP to polysulfone (PSF) casting

14   solution caused the formation of finger-like structure improving the porosity of the membrane

15   and enhancing both the gas-liquid contact area and the CO_2 absorption flux. It can be stated

16   that both the pore size and porosity exerted a major effect on CO_2 absorption flux of COP

17   membranes. For instance, the CO_2 absorption flux of PEG-modified membranes having less

18   mean pore size and high porosity was comparable to that of the membrane M-Span-A having

19   a greater mean pore size but a lower porosity.

20   For the side B configuration test, the CO_2 absorption flux was improved significantly for

21   the membranes M-PEG-A/W and M-Span-A. For both membranes the enhancement of the CO_2

22   absorption flux was about 100% (i.e. 16×10^{-5} mol/m^2.s for both membranes) compared to side

23   A configuration test (7.8×10^{-5} and 7.9×10^{-5} mol/m^2.s for M-PEG-A/W and M-Span-A,

24   respectively). In contrast, the CO_2 absorption flux of the other membranes was maintained

25   almost similar to that of the side A. These results can be explained as follows.

1   In MC, the absorption flux depends on various factors including the morphological

2   structure of the membrane and the process parameters [42]. Based on the resistance-in-series

3   model, the overall mass transfer resistance for CO_2 is the combination of CO_2 transfer

4   resistance from the bulk gas phase to the gas-membrane interface, the resistance to mass

5   transport through the membrane pores, and the resistance from the membrane-liquid interface

6   to the bulk liquid phase [43]. The resistance to gas diffusion from the bulk gas to the membrane

7   interface can be ignored compared to the other resistances [44]. On the other hand, the liquid

8   phase mass transfer resistance is negligible due to the chemical reaction for absorption by the

9   alkaline solution [45]. Therefore, the membrane resistance has a predominant role in MC. In

10   fact, the membrane resistance depends on the morphological structure of the membrane, both

11   skin and sub-layers, together with their characteristics affecting considerably the membrane

12   mass transfer resistance. It was stated that the morphology of the sublayer affected more the

13   rate of mass transfer because the mass transfer through the membrane is solely diffusive

14   mechanism [7]. In the present study, the prepared COP membranes M-NA-A and M-PVP-A/W

15   have an asymmetric structure consisting of a dense top skin layer with a finger-like structure

16   near the top surface and a sponge-like structure near the bottom surface with open and larger

17   pores. It is generally accepted that the finger-like structure provides an easy channel for gas

18   diffusion while the sponge-like structure contributes to a higher mass transfer resistance [46].

19   Although the dense skin layer prevents liquid penetration into the pores, it decreases the contact

20   area between liquid and gas. On the other hand, the bottom side of the membrane (Side B

21   configuration test) having larger and more pores provides more contact area. Nevertheless, the

22   resistance caused by the sponge-like structure exerted more influence on mass transfer rate. As

23   a result, the orientation of the membrane has no considerable effect on the absorption flux of
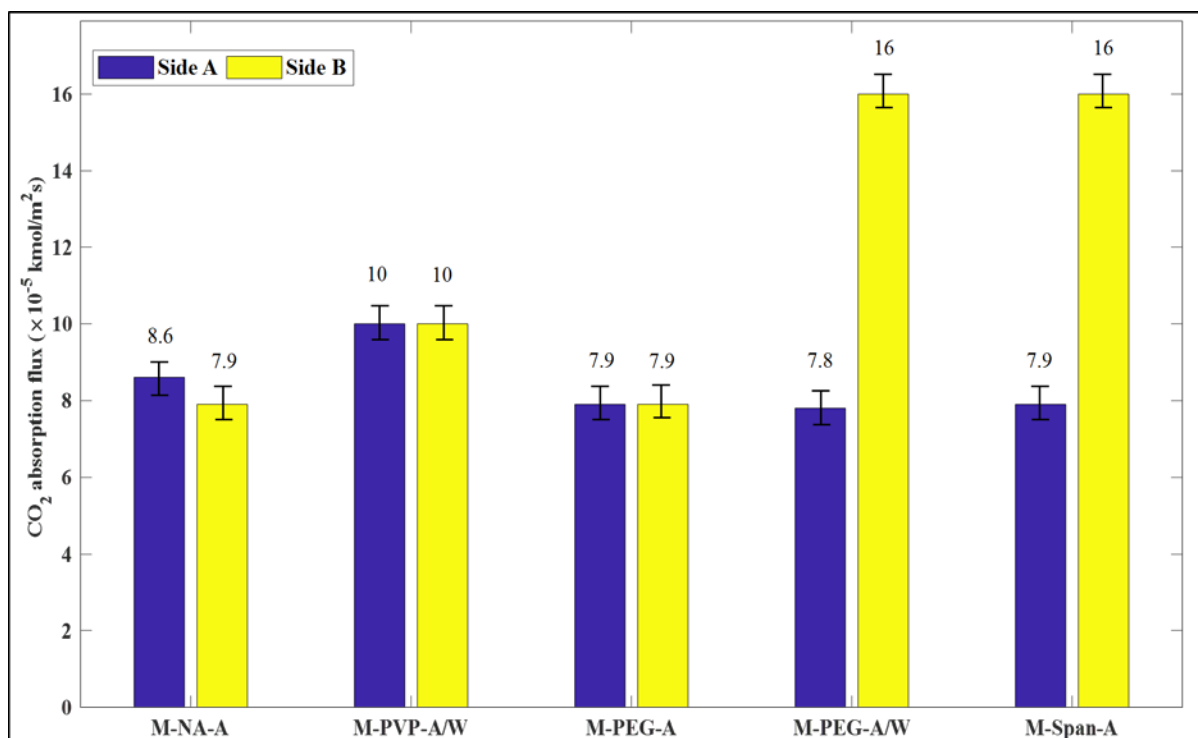
24   these two membranes.

1   Compared to the membranes M-NA-A and M-PVP-A/W, the membrane M-PEG-A has a

2   more homogenous structure (i.e. less finger-like structure and larger pores in the sponge-like

3   structure). As it can be seen in Fig. 7, the absorption flux of the membrane M-PEG-A was

4   almost similar to that of the membrane M-NA-A, but lower than that of the membrane M-PVP-

5   A/W (7.9×10^{-5} mol/m^2.s for M-PEG-A *vs.* 8.6×10^{-5} and 10×10^{-5} mol/m^2.s for M-NA-A and M-

6   PVP-A, side A, respectively). It was mentioned that PEG suppressed macrovoids and resulted

7   in smaller pore sizes compared to the membrane M-PVP-A/W, but almost the same as the pore

8   size of the membrane M-NA-A. Besides, the membrane orientation had no effect on the

9   absorption flux due to the more homogenous cross section structure of the M-PEG-A

10   membrane.

11   The considerable enhancement of the CO_2 absorption flux for the side B of the membranes

12   M-PEG-A/W and M-Span-A compared to that of side A may be related with the big

13   macrovoids observed through the cross-section of these two membranes. Moreover, the M-

14   PEG-A/W membrane had higher porosity and smaller mean pore size (73.3% and 158 nm,

15   respectively, Table 3) while the membrane M-Span-A was less porous with larger mean pore

16   size (50% and 239 nm, respectively, Table 3). It can be concluded that for COP membrane, the

17   morphology of the pores, the presence of big macrovoids in the cross section and the relative

18   disappearance of the sponge-like structure, are more important characteristics for better CO_2

19   absorption flux than some membrane parameters like porosity and pore size. It is worth noting

20   also that larger pores induce a lower gas transport resistance and consequently a greater

21   permeate flux. Furthermore, in some research studies [33, 44] it was reported that a high

22   porosity made the process more efficient. However, the membrane M-Span-A having less

23   porosity showed better performance compared to the membranes M-NA-A, M-PVP-A/W and

24   M-PEG-A (side B, Fig. 7).

1   Wu et al. [38] also investigated the effect of membrane orientation on the membrane

2   contactor performance and claimed that the high CO_2 absorption rate was achieved when the

3   bottom surface faced the water as absorbent due to the more open bottom structure. It was also

4   reported that when a rougher surface was faced the liquid absorbent, the anti-wetting properties

5   enhanced the efficiency of the absorption process. As stated earlier, the roughness parameters,

6   R_a and R_q, of the bottom surface of all COP membranes are greater than those of the top surface.

7   In addition, the bottom surface of the COP membranes showed more and bigger pores (Fig. 5

8   ((a-3)-(e-3)) than those of the top surface. As a result, the particular sublayer morphology of

9   M-PEG-A/W and M-Span-A membranes along with these two positive effects resulted in an

10   enhancement of the CO_2 absorption flux when the side B oriented membranes were used.

11   It is worth mentioning that a continuous test of 250 h was carried out for the two membranes

12   M-PEG-A/W and M-Span-A and no significant decline of the CO_2 absorption flux was

13   detected. The initial CO_2 absorption flux was 1.6×10^{-4} mol/m^2.s for both membranes, while

14   the final CO_2 absorption flux was 1.3×10^{-4} mol/m^2.s and 1.5×10^{-4} mol/m^2.s for M-PEG-

15   A/W and M-Span-A membranes, respectively. This detected reduction was within the

16   registered experimental error.

17

Fig. 7. CO_2 absorption flux of the prepared COP membranes placed in the MC considering the two membrane orientations (Side A and Side B).

For sake of comparison, the MC performance together with some characteristics of commercial and prepared membranes are summarized in Table 5. It is worth quoting that the hollow fiber configuration is the most commonly used type of membrane for MC research applications. Compared to the commercial and prepared MC membranes, the COP membranes showed good features in terms of mean pore size, porosity, contact angle and *LEP* data. The mean pore size of the COP membranes was in the range of 158-265 nm, which is in a good agreement with the pore size of commercial membranes (~ 200 nm). Moreover, the porosity of COP membranes was reasonably high (i.e. greater than 73%), except the membrane M-Span-A, which had a porosity of 50%. As can be seen in Table 5, most of MC membranes had a porosity about 40-50% and only few of them exhibited a porosity greater than 70%. Although COP membranes had a good hydrophobic character, determined by water contact angle (WCA), the hydrophobicity of the membranes presented in Table 5 were better than that of COP membranes except the commercial PVDF membrane. Among all used materials in MC,

32

PTFE has the lowest surface free energy and consequently not only hydrophobic but superhydrophobic membranes were achieved. In general, the proposed COP membranes were suitable in MC applications. The CO_2 absorption flux of the prepared COP membranes in this study was within the range of the claimed values for commercial and developed MC membranes.

Table 5. Membrane characteristics and CO_2 absorption flux of different types of commercial and prepared membranes for MC applications.

Membrane material	Module configuration	$\mu_P{}^a$ (nm)	ε (%)	*LEP*	*WCA* (°)	Absorption flux (mol/m².s)	Absorbent liquid	Test conditions	Ref.
Commercial PTFE[b]	HF[c]	-	~33	-	-	2.7×10^{-4}	Aqueous solutions of MEA (30 wt.%)	Feed: CO_2/N_2 mixtures (15% vol. CO_2) Gas velocity: 0.04m/s	[47]
Commercial PTFE[d]	HF	450	50	-	-	2×10^{-4}	1M AMP[e]	Feed: CO_2/N_2 mixtures (5-10% vol. CO_2) Gas flow rate:16-64 mL/min	[48]
Commercial PTFE[f]	HF	-	50	-	-	25×10^{-4}	2M MEA	Feed: CO_2/air (9% vol. CO_2) Gas flow rate:425L/h Liquid flow rate: ~0.006 m³/h	[49]
PTFE	FS[g]	166	85	-	135.1	1.1×10^{-4}	0.06M MEA	Feed: CO_2/N_2 mixtures (1-9.5% vol.) Liquid flow rate:250 mL/min Gas flow rate:200 mL/min	[50]
Commercial PVDF[h]	HF	200	60	-	-	3.5×10^{-4}	1M MEA	Feed: CO_2/N_2 mixtures (20% vol CO_2) Liquid velocity: 1m/s Gas flow rate:200 mL/min	[51]
Superhydrophobic PTFE[i]	HF	-	45	-	158.4	5.6×10^{-4}	20 wt% K_2CO_3 solution	Feed: biogas (CO_2/ CH_4: 40/60 vol%) Gas flow rate: 500 mL/min Liquid flow rate:75 mL/min P= 1 bar	[52]
Commerical PVDF[j]	HF	200	50	-	96.3	1.3×10^{-4}	1M MDEA	Feed: CO_2/N_2 mixtures (1-15% vol. CO_2) Liquid flow rate: 200 mL/min Gas flow rate: 200 mL/min	[53]
Commerical PP[k]	HF	200	40	-	129.4	$\sim2\times10^{-4}$	1M MDEA	Feed: CO_2/N_2 mixtures (1-15% vol. CO_2) Liquid flow rate: 200 mL/min Gas flow rate: 300 mL/min	[53]
Commerical PP[l] Superhydrophobic PP[l]	HF HF	230 200	- -	-	122 158	$\sim2.3\times10^{-4}$ $\sim1.8\times10^{-4}$	1M MEA 1M MEA	Feed: CO_2/N_2 mixtures (20% vol CO_2) Liquid flow rate: 17 mL/min Gas flow rate: 200 mL/min	[54]

Commerical PP[m]	HF	40	40	-	-	6.1×10^{-5}	ionic liquid[n]	Feed: CO_2/N_2 mixtures (15% vol CO_2) Liquid flow rate: 60 mL/min Gas flow rate: 100 mL/min	[55]
Commerical PP[o]	HF	200	65	-	-	~0.16×10^{-4}	aqueous solutions MDEA (30% wt)	Feed: CO_2/N_2 mixtures (20% vol CO_2) Liquid flow rate: 100 mL/min Gas flow rate: 200 mL/min	[56]
Coated PVDF-silica	FS	78	76	6.2	120	2.84×10^{-4}	1M DEA	Feed: pure CO_2 Liquid flow rate: 100 mL/min Gas flow rate: 100 mL/min	[57]
This study (M-Span-A)	FS	239	50	4.55	100	1.6×10^{-4}	1M MEA	Feed: 15 % (v/v) of CO_2 in N_2 Liquid flow rate: 150 L/h Gas flow rate: 8.4 L/h	

1   [a]: mean pore size
2   [b]: fiber supplier: Polymem (Toulouse, France)
3   [c]: hollow Fiber
4   [d]: supplied by Sumitomo Denko Co., Ltd. (TB-21)
5   e: sterically hindered 2-amino-2-methyl-1-propanol
6   [f]: supplied by Sumitomo Electric Fine Polymer (Japan)
7   [g]: flat Sheet
8   [h]: supplied by Memcor Australia (South Windsor, New South Wales, Australia)
9   [i]: PTFE hollow fiber membrane supplied by DD Water Group Co., Ltd, China
10   [j]: supported from Pall Co. (UMP-0047R)
11   [k]: supported from Pall Co. (LM2P16)
12   [l]: supplied by Tianjin Blue Cross Membrane Technology Co., Ltd., China
13   [m]: mesoporous polypropylene hollow fiber membranes potted with polyurethane supplied by Liqui-Cel [TM], USA.
14   [n]: (1-ethyl-3-methylimidazolium ethylsulfate([emim][EtSO4]))
15   [o]: supplied by GDP Filter Indonesia membrane industry

4   Conclusions

Porous flat-sheet membranes were prepared with a novel and cost effective engineering polymer (COP) via NIPS technique using different additives (PVP, PEG400 and Span 80) and coagulants (acetone with/without water). The study of thermodynamic behavior of COP membranes during phase inversion confirmed the fast solidification process of COP membranes inducing a more porous structure. The addition of PEG and Span resulted in a delayed demixing, suppressing the finger-like structure observed in the membrane structure of the COP membrane prepared without additive and the formation of some big voids. The structural properties of COP membranes showed that the porosity and pore size of the membranes were in the range of 50 - 80% and 158 - 265 nm, respectively. The hydrophobic character of COP membranes was confirmed by the high water contact angle that achieved 111º. The contact angle of the prepared membranes using 1M MEA as a liquid absorbent was found to be in the range 67-73º being the maximum value for the membrane M-Span-A. The *LEP* data (1.67 - 4.55 bar) indicated that the prepared COP membranes can be used in MC applications. The mechanical properties including tensile strength, elongation at break and Young´s modulus lied between 4.53 - 5.15 MPa, 4.08 - 7.94% and 190 - 232 MPa, respectively. These data are comparable with those of the membranes frequently used in MC. The MC performance test carried out using 1M MEA solution as absorbent showed a maximum CO_2 absorption flux of 1.6×10^{-4} mol/m^2.s for COP membranes prepared with PEG and Span 80 additives when the liquid absorbent was brought into contact with their bottom side. The effect of the membrane orientation on CO_2 absorption flux was also investigated and based on the obtained results, the larger pores in contact with the absorbent liquid along with macrovoids in the membrane cross section resulted in better MC performance.

References

[1]   C. A. Scholes, S. E. Kentish, and A. Qader, Membrane gas-solvent contactor pilot plant trials for post-combustion CO_2 capture, *Sep. Purif. Technol.*, 237 (2020) 116470, http://doi.org/10.1016/j.seppur.2019.116470.

[2]   S. Zhao, P. Feron, L. Deng, E. Favre, E. Chabanon, Sh. Yan, J. Hou, V. Chen, H. Qi, Status and progress of membrane contactors in post-combustion carbon capture: A state-of-the-art review of new developments, *J. Memb. Sci.*, 511 (2016) 180–206, http://doi.org/10.1016/j.memsci.2016.03.051.

[3]   E. Drioli, E. Curcio, and G. Di Profio, State of the art and recent progresses in membrane contactors, *Chem. Eng. Res. Des.*, 83 (2005) 223–233, http://doi.org/10.1205/cherd.04203.

[4]   A. Mansourizadeh, Z. Aslmahdavi, A. F. Ismail, and T. Matsuura, Blend polyvinylidene fluoride/surface modifying macromolecule hollow fiber membrane contactors for CO_2 absorption, *Int. J. Greenh. Gas Control*, 26 (2014) 83–92, http://doi.org/ 10.1016/j.ijggc.2014.04.027.

[5]   S. Rajabzadeh, Sh. Yoshimoto, M. Teramoto, M. Al-Marzouqi, Y. Ohmukai, T. Maruyama, and H. Matsuyama, Effect of membrane structure on gas absorption performance and long-term stability of membrane contactors, *Sep. Purif. Technol.*, 108 (2013) 65–73, http://doi.org/10.1016/j.seppur.2013.01.049.

[6]   Y. Zhang and R. Wang, Gas-liquid membrane contactors for acid gas removal: Recent advances and future challenges, *Curr. Opin. Chem. Eng.*, 2 (2013) 255–262, http://doi.org/10.1016/j.coche.2013.03.008.

[7]   G. Bakeri, T. Matsuura, and A. F. Ismail, The effect of phase inversion promoters on the structure and performance of polyetherimide hollow fiber membrane using in gas-liquid contacting process, *J. Memb. Sci.*, 383 (2011) 159–169,

http://doi.org/10.1016/j.memsci.2011.08.048.

[8]   A. Mansourizadeh and A. F. Ismail, Effect of additives on the structure and performance of polysulfone hollow fiber membranes for CO_2 absorption, *J. Memb. Sci.*, 348 (2010) 260–267, http://doi.org/10.1016/j.memsci.2009.11.010.

[9]   K. Simons, K. Nijmeijer, and M. Wessling, Gas-liquid membrane contactors for CO_2 removal, *J. Memb. Sci.*, 340 (2009) 214–220, http://doi.org/10.1016/j.memsci.2009.05.035.

[10]   W. Liang, Y. Chenyang, Zh. Bin, W. Xiaona, Y. Zijun, Zh. Lixiang, Zh. Hongwei, and L. Nanwen, Hydrophobic polyacrylonitrile membrane preparation and its use in membrane contactor for CO_2 absorption, *J. Memb. Sci.*, 569 (2019) 157–165, http://doi.org/10.1016/j.memsci.2018.09.066.

[11]   H. Fashandi, A. Ghodsi, R. Saghafi, and M. Zarrebini, CO_2 absorption using gas-liquid membrane contactors made of highly porous poly(vinyl chloride) hollow fiber membranes, *Int. J. Greenh. Gas Control*, 52 (2016) 13–23, http://doi.org/10.1016/j.ijggc.2016.06.010.

[12]   S. Li, D. J. Rocha, S. James Zhou, H. S. Meyer, B. Bikson, and Y. Ding, Post-combustion CO_2 capture using super-hydrophobic, polyether ether ketone, hollow fiber membrane contactors, *J. Memb. Sci.*, 430 (2013) 79–86, http://doi.org/10.1016/j.memsci.2012.12.001.

[13]   M. Yamazaki, Industrialization and application development of cyclo-olefin polymer, *J. Mol. Catal. A Chem*, 213 (2014) 81–87, http://doi.org/10.1016/j.molcata.2003.10.058.

[14]   W. S. R. Lago, C. Aymes-Chodur, A. P. Ahoussou, and N. Yagoubi, Physico-chemical ageing of ethylene–norbornene copolymers: a review, *J. Mater. Sci.*, 52 (2017) 6879–6904, http://doi.org/10.1007/s10853-017-0925-9.

[15]   P. S. Nunes, P. D. Ohlsson, O. Ordeig, and J. P. Kutter, Cyclic olefin polymers: Emerging materials for lab-on-a-chip applications, *Microfluid. Nanofluidics*, 9 (2010), 145–161, http://doi.org/10.1007/s10404-010-0605-4.

[16]   C. C. Hu, K. R. Lee, R. C. Ruaan, Y. C. Jean, and J. Y. Lai, Gas separation properties in cyclic olefin copolymer membrane studied by positron annihilation, sorption, and gas permeation, *J. Memb. Sci.*, 274 (2006) 192–199, http://doi.org/10.1016/j.memsci.2005.05.034.

[17]   M. Doğu and N. Ercan, High performance cyclic olefin copolymer (COC) membranes prepared with melt processing method and using of surface modified graphitic nano-sheets for H_2/CH_4 and H_2/CO_2 separation, *Chem. Eng. Res. Des.*, 109 (2016) 455–463,

http://doi.org/10.1016/j.cherd.2016.02.021.

[18]   A. A. Shutova, A.N. Trusov, M.V. Bermeshev, S.A. Legkov, M.L. Gringolts, E.Sh. Finkelstein, G.N. Bondarenkom, and A.V. Volkov, Regeneration of alkanolamine solutions in membrane contactor based on novel polynorbornene ,*Oil Gas Sci. Technol. - Rev. d'IFP Energies Nouv.*, 69 (2014) 1059–1068, 2014, Available: https://ogst.ifpenergiesnouvelles.fr/articles/ogst/abs/2014/06/ogst120298/ogst120298.html.

[19] M. Sabzekar, M. Pourafshari Chenar, Z. Maghsoud, M. C. García-Payo ,M. Khayet, Cyclic olefin polymer as a novel membrane material for membrane distillation applications, *J. Memb. Sci.*, 621 (2021) 118845, http://doi.org/10.1016/j.memsci.2020.118845.

[20]   M. Khayet, C. Y. Feng, K. C. Khulbe, and T. Matsuura, Preparation and characterization of polyvinylidene fluoride hollow fiber membranes for ultrafiltration, *Polymer (Guildf).*, 43 (2002) 3879–3890, http://doi.org/10.1016/S0032-3861(02)00237-9.

[21]   M. Essalhi and M. Khayet, Self-sustained webs of polyvinylidene fluoride electrospun nano-fibers: Effects of polymer concentration and desalination by direct contact membrane distillation, *J. Memb. Sci.*, 454 (2014) 133–143, doi: http://doi.org/10.1016/j.memsci.2013.11.056.

[22] K. L. W. T. D. Wang, Porous PVDF asymmetric hollow fiber membranes prepared with the use of small molecular additives, *J. Membr. Sci.*, 178 (2000) 13-23, https://doi.org/10.1016/S0376-7388(00)00460-9.

[23] S. Mohsenpour, A. Khosravanian, Influence of additives on the morphology of PVDF membranes based on phase diagram: Thermodynamic and experimental study, *J. Appl. Polym. Sci.*, 135 (2018) 46225, https://doi.org/10.1002/app.46225.

[24]   M. J. Han and S. T. Nam, Thermodynamic and rheological variation in polysulfone solution by PVP and its effect in the preparation of phase inversion membrane, *J. Memb. Sci.*, 202 (2002) 55–61, https://doi.org/10.1016/S0376-7388(01)00718-9.

[25]   N. Nabian, A. A. Ghoreyshi, A. Rahimpour, and M. Shakeri, Performance evaluation and mass transfer study of CO_2 absorption in flat sheet membrane contactor using novel porous polysulfone membrane, *Korean J. Chem. Eng.*, 32 (2015) 2204–2211, https://doi.org/10.1007/s11814-015-0027-9.

[26]   I. C. Kim and K. H. Lee, Effect of poly(ethylene glycol) 200 on the formation of a polyetherimide asymmetric membrane and its performance in aqueous solvent mixture permeation, *J. Memb. Sci.*, 230 (2004) 183–188, https://doi.org/10.1016/j.memsci.2003.11.002.

[27] S. Bonyadi and T. S. Chung, Flux enhancement in membrane distillation by fabrication of dual layer hydrophilic-hydrophobic hollow fiber membranes, *J. Memb. Sci.*, 306 (2007) 134–146, https://doi.org/10.1016/j.memsci.2007.08.034.

[28] Q. Ge, L. Ding, T. Wu, G. Xu, F. Yang, and M. Xiang, Effect of surfactant on morphology and pore size of polysulfone membrane, *J. Polym. Res.*, 25 (2018) 1–13, https://doi.org/10.1007/s10965-017-1410-5.

[29] S. Nejati, C. Boo, C. O. Osuji, and M. Elimelech, Engineering flat sheet microporous PVDF films for membrane distillation, *J. Memb. Sci.*, 492 (2015) 355–363, https://doi.org/10.1016/j.memsci.2015.05.033.

[30] A. Behboudi, S. Ghiasi, T. Mohammadi, M. Ulbricht, Preparation and characterization of asymmetric hollow fiber polyvinyl chloride (PVC) membrane for forward osmosis application, *Sep. Purif. Technol.* 270 (2021) 118801, https://doi.org/10.1016/j.seppur.2021.118801.

[31] F.Ch. Lin, D.M. Wang, Ch.L. Lai, J.Y. Lai, Effect of surfactants on the structure of PMMA membranes, *J. Memb. Sci.* 123 (1997) 281-291, https://doi.org/10.1016/S0376-7388(96)00243-8.

[32] Z. Rezaiyan, P. Keshavarz , M. Khorram, Experimental investigation of the effects of different chemical absorbents on wetting and morphology of poly(vinylidene fluoride) membrane, *J. Appl. Polym. Sci.* (2017) 1-8, https://doi.org/10.1002/app.45543.

[33] S. Atchariyawut, C. Feng, R. Wang, R. Jiraratananon, and D. T. Liang, Effect of membrane structure on mass-transfer in the membrane gas-liquid contacting process using microporous PVDF hollow fibers, *J. Memb. Sci.*, 285 (2006) 272–281, http://doi.org/10.1016/j.memsci.2006.08.029.

[34] H. Matsuyama, T. Maki, M. Teramoto, and K. Kobayashi, Effect of PVP additive on porous polysulfone membrane formation by immersion precipitation method, *Sep. Sci. Technol.*, 38 (2003) 3449–3458, http://doi.org/10.1081/SS-120023408.

[35] Y. C. Zuo, X. Y. Chi, Z. L. Xu, and X. J. Guo, Morphological controlling of CTA forward osmosis membrane using different solvent-nonsolvent compositions in first coagulation bath, *J. Polym. Res.*, 24 (2017)1–15, http://doi.org/10.1007/s10965-017-1311-7.

[36] Y. Zhang, R. Wang, L. Zhang, and A. G. Fane, Novel single-step hydrophobic modification of polymeric hollow fiber membranes containing imide groups: Its potential for membrane contactor application, *Sep. Purif. Technol.*, 101 (2012) 76–84,

1   http://doi.org/10.1016/j.seppur.2012.09.009.

[37] H. A. Tsai, D. H. Huang, R. C. Ruaan, and J. Y. Lai, Mechanical properties of asymmetric polysulfone membranes containing surfactant as additives, *Ind. Eng. Chem. Res.*, 40 (2001) 5917–5922, http://doi.org/10.1021/ie010026e.

[38] X. Wu, B. Zhao, L. Wang, Zh. Zhang, H. Zhang, X. Zhao, X. Guo, Hydrophobic PVDF/graphene hybrid membrane for CO_2 absorption in membrane contactor, *J. Memb. Sci.,* 520 (2016) 120–129, https://doi.org/10.1016/j.memsci.2016.07.025.

[39] A.L. Ahmad, W.K.W. Ramli, Hydrophobic PVDF membrane via two-stage soft coagulation bath system for membrane gas absorption of CO_2, *Sep. Purif. Technol.* 103 (2013) 230–240, https://doi.org/10.1016/j.seppur.2012.10.032.

[40] N. Pezeshk, D. Rana, R.M. Narbaitz, T. Matsuura, Novel modified PVDF ultrafiltration flat-sheet membranes, *J. Memb. Sci.*, 389 (2012) 280–286, http://doi.org/10.1016/j.memsci.2011.10.039

[41] A. Mansourizadeh and A. F. Ismail, Preparation and characterization of porous PVDF hollow fiber membranes for CO_2 absorption: Effect of different non-solvent additives in the polymer dope, *Int. J. Greenh. Gas Control*, 5 (2011) 640–648, http://doi.org/ 10.1016/j.ijggc.2011.03.009.

[42] S. Khaisri, D. deMontigny, P. Tontiwachwuthikul, and R. Jiraratananon, Comparing membrane resistance and absorption performance of three different membranes in a gas absorption membrane contactor,*Sep. Purif. Technol.*, 65 (2009) 290–297, http://doi.org/10.1016/j.seppur.2008.10.035.

[43] V. Y. Dindore, D. W. F. Brilman, R. H. Geuzebroek, and G. F. Versteeg, Membrane-solvent selection for CO_2 removal using membrane gas-liquid contactors, *Sep. Purif. Technol.*, 40 (2004)133–145, http://doi.org/10.1016/j.seppur.2004.01.014.

[44] H. A. Rangwala, Absorption of carbon dioxide into aqueous solutions using hollow fiber membrane contactors, *J. Memb. Sci.*, 112 (1996) 229–240, http://doi.org/10.1016/0376-7388(95)00293-6.

[45] J. L. Li and B. H. Chen, Review of CO_2 absorption using chemical solvents in hollow fiber membrane contactors, *Sep. Purif. Technol.*, 41 (2005) 109–122, http://doi.org/ 10.1016/j.seppur.2004.09.008.

[46] R. Naim, A. F. Ismail, and A. Mansourizadeh, Effect of non-solvent additives on the structure and performance of PVDF hollow fiber membrane contactor for CO_2 stripping, *J. Memb. Sci.*, 423–424 (2012) 503–513, http://doi.org/10.1016/j.memsci.2012.08.052.

[47]   E. Chabanon, D. Roizard, and E. Favre, Membrane contactors for postcombustion carbon dioxide capture: A comparative study of wetting resistance on long time scales, *Ind. Eng. Chem. Res.*, 50 (2011) 8237–8244, http://doi.org/10.1021/ie200704h.

[48]   K. Shimada, I. N. Seekkuarachchi, and H. Kumazawa, Absorption of CO_2 into aqueous solutions of sterically hindered methyl aminoethanol using a hydrophobic microporous hollow fiber contained contactor, *Chem. Eng. Commun.*, 193 (2006) 38–54, http://doi.org/10.1080/009864490923484.

[49]   D. deMontigny, P. Tontiwachwuthikul, and A. Chakma, Using polypropylene and polytetrafluoroethylene membranes in a membrane contactor for CO_2 absorption, *J. Memb. Sci.*, 277 (2006) 99–107, http://doi.org/10.1016/j.memsci.2005.10.024.

[50]   S. C. Chen, S. H. Lin, R. Der Chien, Y. H. Wang, and H. C. Hsiao, Chemical absorption of carbon dioxide with asymmetrically heated polytetrafluoroethylene membranes, *J. Environ. Manage.*, 92 (2010) 1083–1090, http://doi.org/10.1016/j.jenvman.2010.08.014.

[51]   W. Rongwong, R. Jiraratananon, and S. Atchariyawut, Experimental study on membrane wetting in gas-liquid membrane contacting process for CO_2 absorption by single and mixed absorbents, *Sep. Purif. Technol.*, 69 (2009) 118–125, http://doi.org/10.1016/j.seppur.2009.07.009.

[52]   Y. Li, L. Wang, X. Hu, P. Jin, and X. Song, Surface modification to produce superhydrophobic hollow fiber membrane contactor to avoid membrane wetting for biogas purification under pressurized conditions, *Sep. Purif. Technol.*, 194 (2018) 222–230, http://doi.org/10.1016/j.seppur.2017.11.041.

[53]   S. H. Lin, C. F. Hsieh, M. H. Li, and K. L. Tung, Determination of mass transfer resistance during absorption of carbon dioxide by mixed absorbents in PVDF and PP membrane contactor, *Desalination*, 249 (2009) 647–653, http://doi.org/10.1016/j.desal.2008.08.019.

[54]   Y. Lv, X. Yu, J. Jia, S. T. Tu, J. Yan, and E. Dahlquist, Fabrication and characterization of superhydrophobic polypropylene hollow fiber membranes for carbon dioxide absorption, *Appl. Energy*, 90 (2012) 167–174, http://doi.org/10.1016/j.apenergy.2010.12.038.

[55]   S. Qazi, L. Gómez-Coma, J. Albo, S. Druon-Bocquet, A. Irabien, and J. Sanchez-Marcano, CO_2 capture in a hollow fiber membrane contactor coupled with ionic liquid: Influence of membrane wetting and process parameters, *Sep. Purif. Technol.*, 233 (2019) 115986, http://doi.org/10.1016/j.seppur.2019.115986.

[56]   Y. Rahmawati, S. Nurkhamidah, S. Susianto, N. I. Listiyana, M. A. Rahmatullah, and I. M. Hardian, Effect of activated alkanolamine for CO_2 absorption using hollow fiber membrane contactor, *IOP Conference Series Materials Science and Engineering*, (2019) 543: 012080, http://doi.org/10.1088/1757-899X/543/1/012080.

[57]   A. Rosli, N. F. Shoparwe, A. L. Ahmad, S. C. Low, and J. K. Lim, Dynamic modelling and experimental validation of CO_2 removal using hydrophobic membrane contactor with different types of absorbent, *Sep. Purif. Technol.*, 219 (2019) 230–240, http://doi.org/10.1016/j.seppur.2019.03.030.